1A.3

REALTIME HIGH-RESOLUTION MESOSCALE MODELING FOR THE DEFENSE THREAT REDUCTION AGENCY

David R. Stauffer[1*], Glenn K. Hunter[1], Aijun Deng[1], Jeff Zielonka[1],
Kyle Dedrick[2], Charlie Broadwater[2], Andy Grose[2],
Charles Pavloski[1], and Joshua Toffler[2]
[1]Pennsylvania State University, University Park, PA
[2] Defense Threat Reduction Agency, Ft. Belvoir, VA

1. INTRODUCTION

Penn State provides research and development (R&D) support to the Defense Threat Reduction Agency (DTRA) for the Penn State - DTRA in-house mesoscale modeling system while also running parallel mesoscale model forecasts on a mirror computer cluster at Penn State for important worldwide events (e.g., Beijing Summer Olympics). Mesoscale model forecasts are used to drive the HPAC-SCIPUFF atmospheric transport and dispersion (AT&D) model for hazard prediction and consequence assessment. Local and regional scale atmospheric conditions strongly influence atmospheric transport and dispersion (AT&D) processes in the boundary layer, and the extent and spread of dangerous materials in the lower levels of the atmosphere. Managing the consequences of chemical, biological, radiological and nuclear (CBRN) incidents requires detailed knowledge of current and future weather conditions to accurately model potential effects.

DTRA has been running a high-resolution (to ~1-km horizontal resolution) MM5 modeling system in-house since 2005 for support of the 2006 Torino Winter Olympics while Penn State runs that system locally in realtime (Stauffer et al. 2006, Stauffer et al. 2007a, Stauffer et al. 2007b). Penn State has also been running a high-resolution version of the WRF-ARW locally in realtime since 2005. This paper presents some recent examples of realtime high-resolution mesoscale-model and AT&D forecasts, and also compares results from the realtime MM5 and WRF-ARW forecasts for select cases during the 2008 Beijing Summer Olympics.

2. THE PENN STATE – DTRA RELOCATABLE ON-DEMAND FORECAST SYSTEM (ROFS)

Short-range, high-resolution numerical weather prediction (NWP) products are attractive for providing the type of timely weather inputs needed to utilize AT&D models for hazard prediction and consequence assessment. The regional coverage and concentration levels caused by a CBRN incident can contribute to the planned course of action for local authorities and decision makers. A rapidly relocatable on- demand forecast system (ROFS) was designed and implemented at DTRA by Penn State in 2005, and it has been used for reachback support since the 2006 Torino Winter Olympics (Stauffer et al. 2007a).

The ROFS design is patterned after that of the automated, rapidly relocatable nowcast-prediction system (RRNPS) based on the Penn State / NCAR Mesoscale MM5 (Grell et al. 1995) and used by the United States military on the battlefield (Schroeder et al. 2006, Stauffer et al. 2007b). The DTRA ROFS is generally used to produce in-house high-resolution numerical forecasts. Explicit prognostic equations are used for mixing ratios of cloud and water/ice and rain/snow on all domains, while sub-grid deep convection is parameterized (Kain and Fritsch 1990, Kain 2004) on the coarser domains. Turbulence is represented on all grids using a 1.5-order closure, which explicitly predicts turbulent kinetic energy (TKE; Shafran et al. 2000, Stauffer et al. 1999). More details on the model physics may be found in Schroeder et al. (2006).

This DTRA in-house NWP system is designed to use global model initialization from Global Forecast System (GFS) data, and it can also perform mesoscale initialization using a “running start” data assimilation / dynamic initialization (Stauffer et al. 2007a, Stauffer et al. 2007b). The ROFS is designed to run on-demand or on a regular schedule for anywhere in the world while providing the user the flexibility to define the number of domains and domain sizes, the horizontal and vertical resolutions, etc. It also allows for multiple theaters to be run simultaneously on a single massively parallel computing platform. Penn State and DTRA designed and built two identical 22-node Linux clusters, with 88 CPUs per cluster, optimized for DTRA’s needs. An identical 22-node cluster is located at Penn State allowing for continuing software and hardware developments to the MM5 NWP system. This mirror version of the ROFS allows for relatively seamless upgrades to be made to the DTRA in-house systems by Penn State.

The ROFS NWP system is highly automated but designed with the flexibility to modify the model configuration so that domain sizes and resolutions can be easily re-defined to enable outputs to be made available within specified time parameters. For example, one test application for the Beijing Olympics was that the ROFS model output for 36-h forecasts be created within 6 hours of the National Centers for

Corresponding author address: David R. Stauffer, Department of Meteorology, 503 Walker Building, Pennsylvania State University, University Park, PA 16802-5013, email: stauffer@meteo.psu.edu

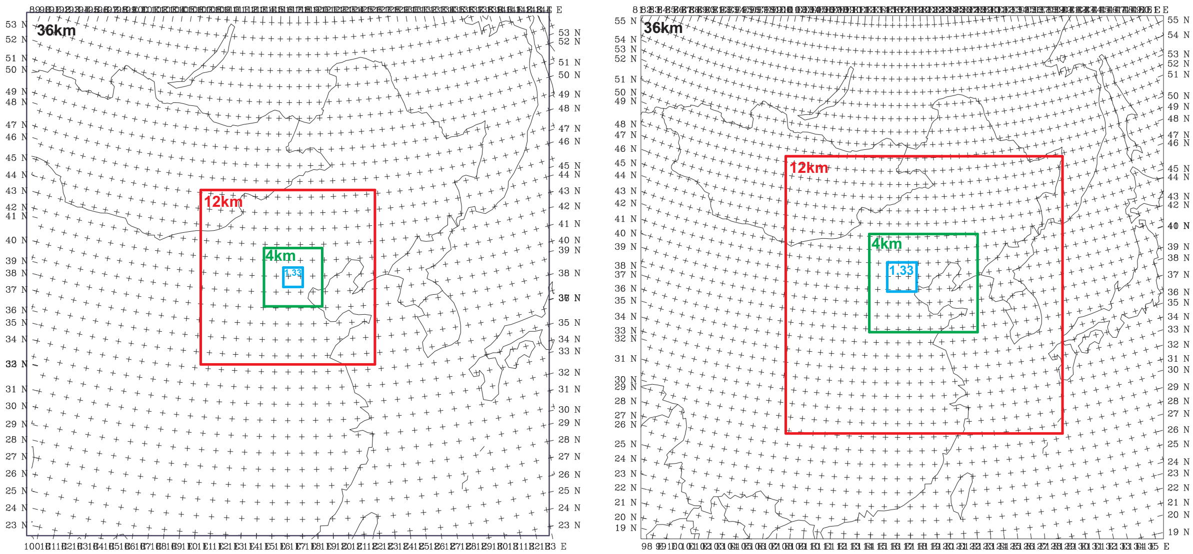

Figure 1. The small and large 4-domain model configurations used for reachback modeling support during the Beijing Summer Olympics.

Environmental Prediction (NCEP) GFS model-initialization valid time. Since the GFS data are generally not available for processing until 3.5 to 4 hours after valid time, the model had only approximately 2 to 2.5 hours to produce its high-resolution outputs. For the Beijing Olympics, there was the added challenge that some of the venues were displaced as far as Hong Kong for some equestrian events. Since the NWP cluster configuration allows multiple theaters to execute simultaneously, DTRA, under the guidance of Penn State, ran two sets of 36-h forecasts using two different domain size configurations (Fig. 1). The smaller configuration allowed a complete set of domains with 36-km, 12-km, 4-km and 1.3-km horizontal grid resolutions to be run within the allotted time frame, utilizing half of the cluster's nodes for each set of domains. The larger configuration encompassed all the Olympic venues and allowed an expanded domain size configuration to better resolve the coastal regions and Yellow Sea while still providing output at 4-km resolution within the allotted time frame. The larger 1.3-km domain was still available within 12 hours past the GFS valid time. Model results from the large and small domain configurations were statistically comparable for most cases (not shown). The focus here will be on the large-domain results.

The DTRA in-house ROFS is typically run off of an automated scheduler (via crontab) but may also be run in a manual mode. It can also be used in a historical mode to rerun domains or reconfigured domains when necessary. The ROFS domains are run sequentially and one-way nested, which allows more ready access to the model data because data may be used from the already completed coarser domains as the finer domains are still executing. The start times of the nested domains may also be offset or lagged with that of the mother mesh to allow larger domain sizes and greater efficiency by overlapping the data ingest / processing with the model computations. The weather model outputs, instantaneous or temporally averaged, are then converted into special format "MEDOC" files that are utilized by the HPAC/SCIPUFF AT&D system (Sykes et al. 2006).

3. SAMPLE REALTIME ROFS RESULTS

Penn State provided 36-h ROFS forecasts for realtime test applications at 36-km, 12-km, 4-km and 1.3-km resolutions. A web page created at Penn State provided 24/7 access to graphical and digital (GRIB) meteorological model outputs for these events. An important feature of the DTRA ROFS NWP system is its ability to create high-resolution meteorological fields in regions of complex terrain. For example, to obtain realistic sea breeze circulations occurring just to the east of Beijing, it was important to resolve the Yellow Sea and the detailed coastline with the 4-km domain. As seen in Fig. 2, the series of bays and peninsulas in this area can create a highly complex wind pattern during the early afternoon period. The 30-h forecast of surface-layer wind shows very good agreement with the local surface wind observations. The wind flow is diverted towards the different shores due to the differential daytime heating between the land (green) and the water (white).

An example of the ROFS multiple-theater functionality Is shown in Fig. 3 with a domain centered in Minnesota and the arrival of Hurricane Gustav to the Gulf Coast. While the Louisiana coastline was still captured by the Minnesota domain configuration (within its outer 36-km domain), it included only part of the Gulf of Mexico. The Hurricane Gustav landfall location was well-predicted and occurred around 15 UTC (0900 local standard time (LST)) as observed. However, the storm

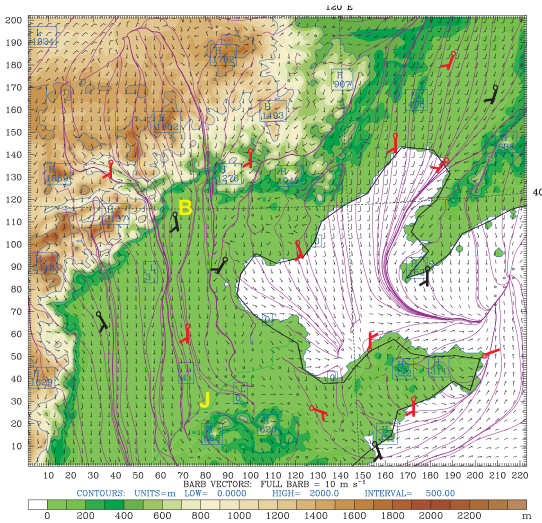

Figure 2. The 30-h surface-layer wind forecast of model-predicted streamlines and gridded winds barbs demonstrating sea-breeze effects on the large 4-km Beijing domain flow fields at 06 UTC (1400 LST) 9 August 2008. Heavy black barbs denote standard WMO surface wind observations used in the statistical analysis presented in Section 5, and red barbs indicate supplemental surface wind observations. B is Beijing and J is Jinan.

had only recently entered the 36-km domain from the GFS lateral boundary condition and with the limited stretch across the warm waters, the central pressure was predicted as only 984 hPa (Fig. 3a) compared to the observed value of 955 hPa.

A secondary set of domains centered over the southern coast of Louisiana based on the projected track by the National Hurricane Center was easily created at Penn State to better model Gustav's landfall. The central pressure of Gustav was then forecasted on the 36-km domain to be 21 hPa lower or 963 hPa (Fig. 3b). Since the domains were re-centered, the landfall was also captured by the 12-km, 4-km, and 1.3-km domains. Use of higher model resolution created the improved intensity forecast as shown by the 4-km and 1.3-km forecasts in Fig. 4.

Another example of the complexity of the observed and predicted wind flows in complex terrain can be demonstrated by placing a nested 1.3-km domain at the front range of the Rockies. During the early evening / nighttime hours downslope / channeling flows appeared along the Rocky Mountains in Colorado (Fig. 5). In this example, one can see that the 1.3-km domain produces westerly downslope flows and accurately depicts its extent around the NCAR Mesa Lab (denoted by the letter M), while Denver (denoted by the letter D) is experiencing the larger-scale northerly flow behind a surface trough further to the east. The interaction of these two flow patterns results in a well-defined confluence zone (heavy dashed line). The positioning of this confluence zone matches well with the WMO surface wind observations in red. In these cases, these finer resolution domains are critically important to resolve the flows influenced by complex terrain and coast lines that affect local AT&D and thus the hazard prediction and consequence assessment of CBRN releases.

a)

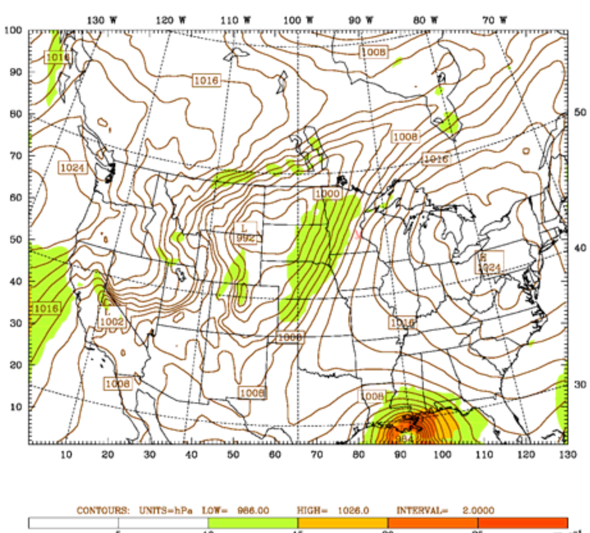

b)

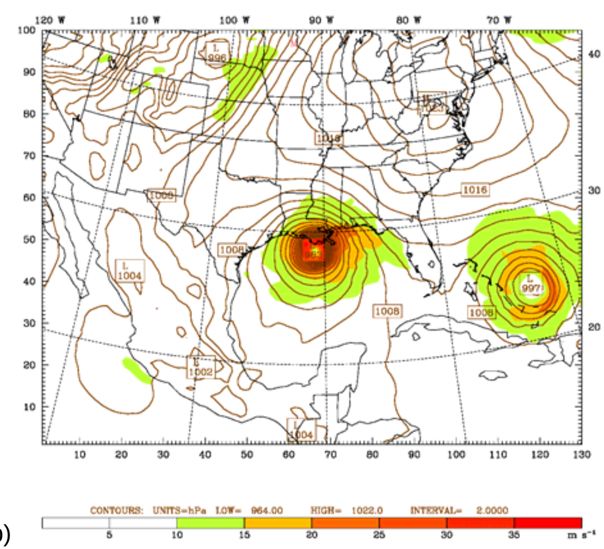

Figure 3. The 27-h forecasts of landfalling Hurricane Gustav at 15 UTC (0900 LST) 1 September 2008 on the Minnesota-centered 36-km domain (left) and Gulf Coast / Louisiana-centered 36-km domain (right). Contours are sea-level pressure (hPa) and color shading indicates wind speed (ms^{-1}, key at bottom).

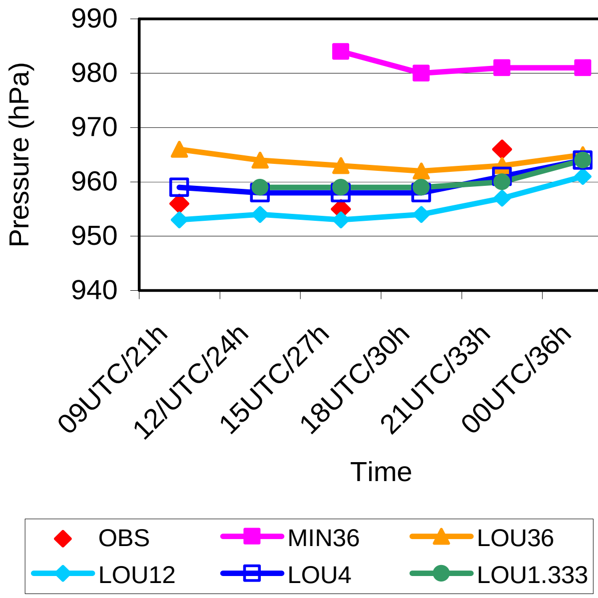

Figure 4. Time series of observed and predicted central pressure (hPa) of Hurricane Gustav as a function of model resolution and domain center. The large red diamonds represent the observed central pressure. The upper-most line shows the 36-km forecast from the Minnesota (MIN) domain configuration. The lower four lines show the forecasted pressures for the domain centered over Louisiana (LOU) at 36-km, 12-km, 4-km, and 1.3-km resolutions, respectively.

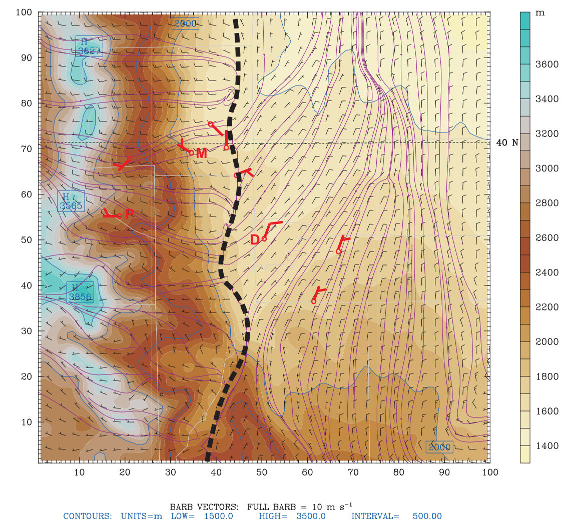

Figure 5. The 3-h surface wind forecast over Colorado on the 1.3-km nested domain valid at 03 UTC (2000 LST) 2 September 2008 demonstrating early-evening downslope and channeling winds from the Rocky Mountains. Note the confluence line (heavy dashed line) separating the region of downslope flow (west of the confluence line) interacting with the large scale flow (east of the confluence line). P is Prospector's Run, D is Denver, and M is Mesa Lab at NCAR.

4. SAMPLE HPAC-SCIPUFF RESULTS USING ROFS WEATHER INPUTS

Some examples of HPAC-SCIPUFF predictions using the realtime ROFS weather inputs shown above are presented to demonstrate the details afforded to the AT&D predictions from the high-resolution meteorological inputs.

Figure 6 shows 12-h surface dosages from three releases initiated at 00 UTC (0800 LST) 9 August 2008 at the three different locations depicted by triangles. A 3-h release was made over the Yellow Sea where it would interact with the multiple flow features created by the interaction of the sea breeze with the complex coastline, a 1-h release was initiated over Jinan in the southern part of the domain and largely in the plains, and another 1-h release was defined over Beijing, which was located just upwind from the mountainous region to the north. All three plumes produced surface dosages that spread very differently in their horizontal paths, as suggested by the complex surface flows during this daytime period in Fig. 2 above. The Yellow Sea plume spreads in multiple directions due to the complex sea breeze, the Jinan plume moves in a north-northwesterly direction, and the Beijing plume fans outwards as it advects into the higher terrain. Vertical cross sections through the three atmospheric plumes at 3, 6, 9 and 12 h (not shown) indicate varying vertical extents through this daytime period with the Yellow Sea plume staying mainly in the lowest 1000 m MSL, the Jinan plume reaching 3000 m MSL and the Beijing plume passing through 5000 m MSL as it moves upslope.

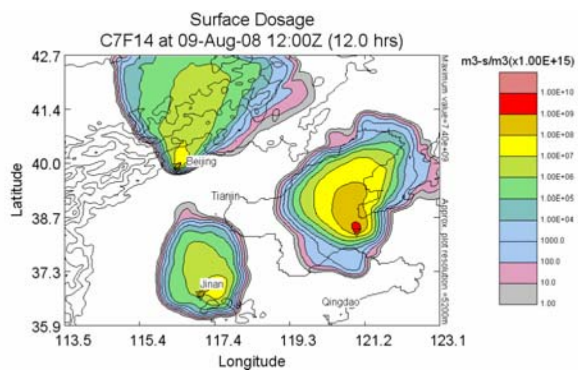

Figure 6. The 12-h SCIPUFF prediction of surface dosage at 12 UTC (2000 LST) 9 August 2008 caused by early-morning plumes caused by releases at Beijing, Jinan and over the Yellow Sea. Compare this figure with Fig. 2, the daytime-predicted surface flow patterns at 06 UTC (1400 LST) midway through the 12-h period. Surface dosages are indicated by the color key to the right of the figure, and each release location is indicated by a triangle.

The importance of the surface confluence zone predicted east of the Rocky Mountains and west of Denver Colorado in Fig. 5 above can be readily seen in the surface concentration predictions in Fig. 7. Three late afternoon (00 UTC / 1700 LST) releases were initiated at the locations indicated in Fig. 5 straddling the confluence zone predicted 3 h later at 03 UTC (2000 LST). The 1.3-km ROFS domain allowed for very accurate placement of the confluence line along the front range of the Rockies. The confluence line, created

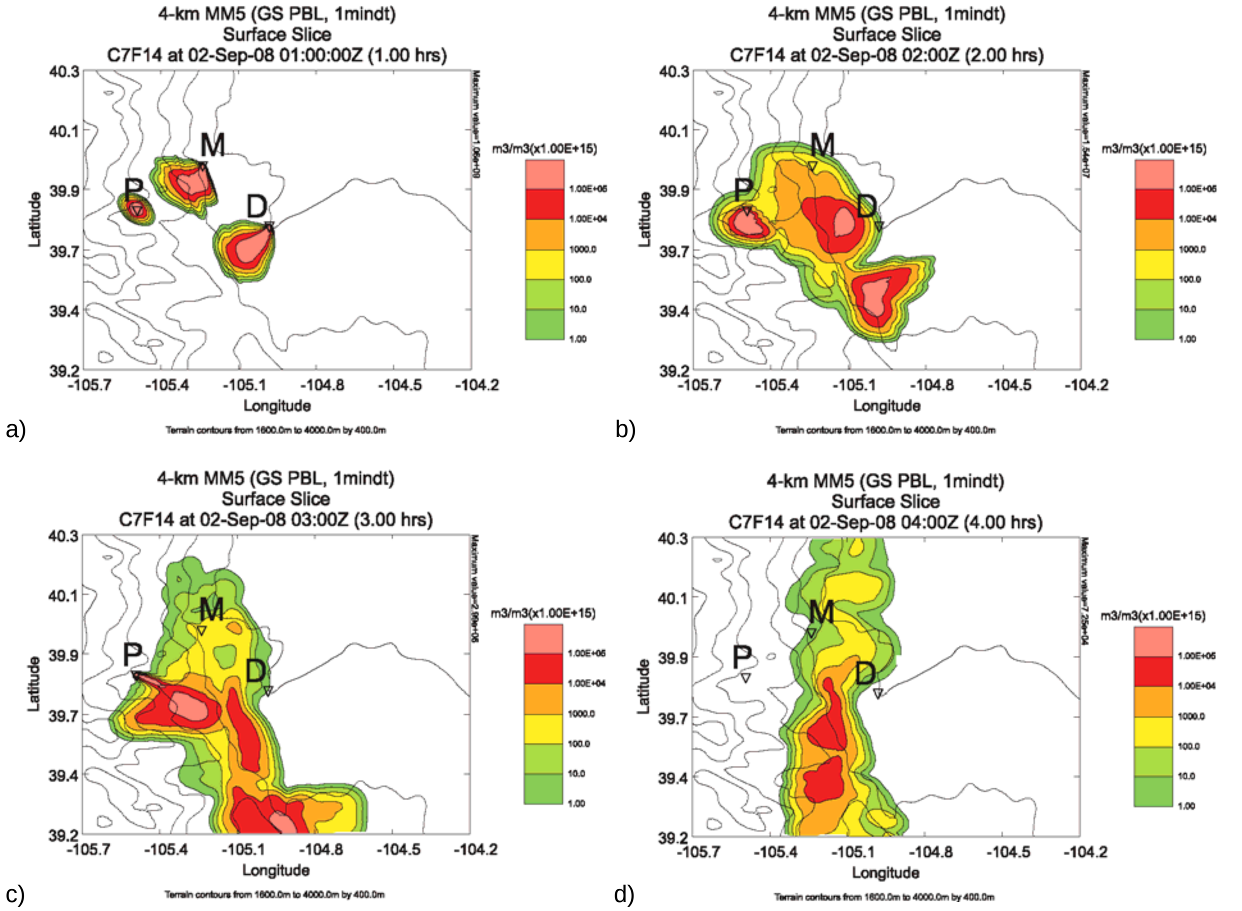

Figure 7**.** The SCIPUFF-predicted surface-layer concentrations (concentration values in key to the right of each figure) in the region of the confluence zone at 1, 2, 3 and 4 h following the initial releases at 00 UTC (1700 LST) 2 September 2008. The releases were initiated at Prospector's Run (P), Denver (D), and Mesa Lab at NCAR (M). Compare with surface wind forecast and confluence line at 3 h in Fig. 5.

by downslope flow to the west and the larger-scale flow to the east, produced a path to funnel the plumes along this axis of the confluent deformation. SCIPUFF-predictions are shown at intervals of 1 h following the initial release time to 1 h after the surface wind forecast shown in Fig. 5. Note that the westerly flow from the mountains appears to spread eastward with time (plumes at 1 h reflect mainly easterly flow) and it should be noted at 03 UTC, the 1.3-km domain's depiction of the highly resolved terrain shows some of the plume filling into the adjacent valley. By 04 UTC (2100 LST), the combined surface plumes become oriented north-south along the surface confluence zone. Thus meteorological details such as these related to terrain forcing and model resolution can play a very important role in AT&D forecasts for hazard prediction and consequence assessment.

5. MM5 ROFS – WRF COMPARISONS FOR THE BEIJING OLYMPICS

MM5 and WRF-ARW were run twice daily (00 and 12 UTC) for R&D support of the 2008 Beijing Summer Olympics (8 August – 24 August 2008). MM5 was run with both the standard 100 X 100 X 30 domain configuration and the expanded, large-domain configuration as shown in Fig. 1. WRF was run only at Penn State with the large-domain configuration. The PSU-DTRA ROFS forecasts based on MM5 are compared with the WRF-ARW forecasts produced at Penn State using the same domain configuration and similar physics options for a subset of six diverse cases described in Table 1. Case 1, the monsoon/sea-breeze case, was presented in previous sections. These six cases were picked to represent the full range of model performance using the case-by-case statistics for the entire Olympics period.

The 36-km, 12-km and 4-km MM5 and WRF forecasts are statistically compared over the large 4-km domain area in Fig. 1. Since only two or three WMO sonde locations were available on average for each case over the 4-km domain and only one sonde (Beijing) is available on the 1.3-km domain, no verification is presented for the 1.3-km domains. The models are also configured with comparable model physics. The MM5 uses the Penn State (GS) TKE-predicting turbulence scheme while the WRF-ARW uses a version of the MYJ TKE-predicting scheme modified to

.Case Number	Dates	Description
1	08 Aug 2008, 00 UTC – 09 Aug 2008, 12 UTC	Monsoon/Sea Breeze
2	10 Aug 2008, 00 UTC – 11 Aug 2008, 12 UTC	Siberian System / Monsoon Interaction
3	12 Aug 2008, 12 UTC – 14 Aug 2008, 00 UTC	Hot and Muggy with Showers
4	13 Aug 2008, 12 UTC – 15 Aug 2008, 00 UTC	Disorganized Convection
5	19 Aug 2008, 00 UTC – 20 Aug 2008, 12 UTC	Hot and Dry
6	20 Aug 2008, 12 UTC – 22 Aug 2008, 00 UTC	Frontal Precipitation

Table 1. Six-case subset of 36-h forecasts chosen from the Beijing Olympics period (8 – 24 August 2008) for MM5 and WRF comparisons

reduce the positive bias in PBL height by adopting a diagnosis method based on that in the GS scheme and reducing the background value for TKE (Reen et al. 2008, Zielonka et al. 2008). Both models use the updated Kain-Fritsch 2 convective parameterization, the same longwave and shortwave radiation schemes, and similar simple-ice (no mixed phases) microphysics. Both are run without data assimilation and use force-restore / thermal diffusion for the land-surface model.

5.1 Meteorological results for the six Beijing cases

The MM5- and WRF-predicted MAE values for surface-layer wind speed, wind direction and temperature verified over the 4-km domain area for the 36-km, 12-km and 4-km grid predictions, averaged over the 36-h forecast periods for the six Beijing Olympics cases (Table 1), are shown in Fig. 8. These figures show that overall WRF has somewhat smaller errors in the predicted wind speed and somewhat larger errors in the temperature field. The results are mixed for surface wind direction with MM5 performing better than WRF for some cases and WRF performing better than MM5 for other cases.

The comparisons of MM5- and WRF-predicted profiles of MAE verified over the 4-km domain area for the 36-km, 12-km and 4-km grid predictions averaged over the 36-h forecast periods for the six Beijing Olympics cases (Table 1) are shown in Fig. 9 (wind speed), Fig. 10 (wind direction) and Fig. 11 (temperature). In general, WRF had lower surface and boundary layer wind speed errors, and MM5 had lower surface and boundary layer temperature errors. Wind direction errors were comparable between the two models with WRF performing slightly better in the

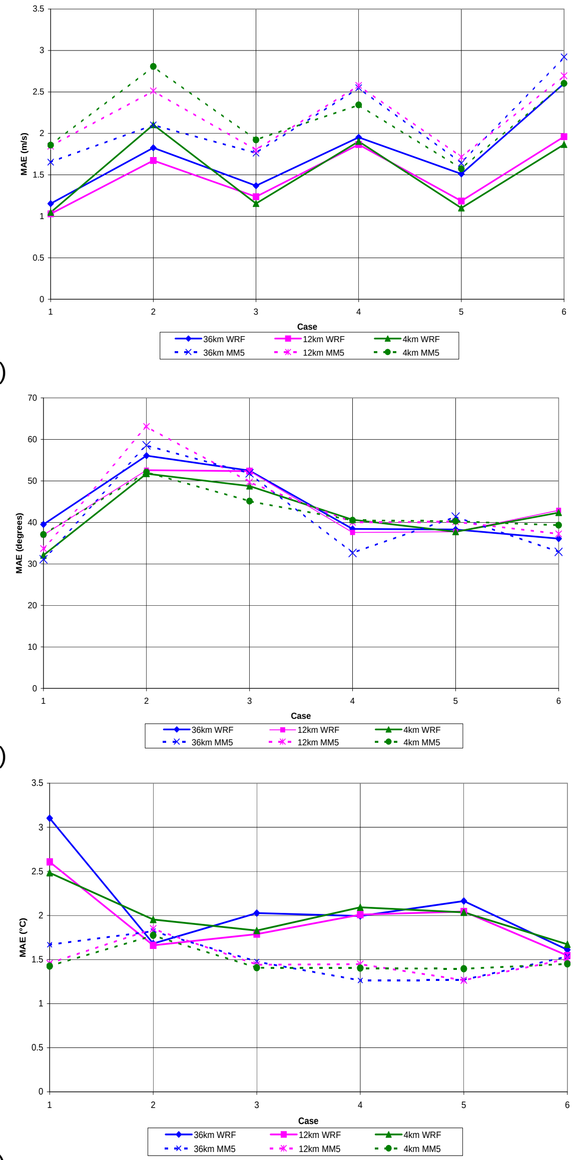

a)
b)
c)

Figure 8. Comparison of MM5- and WRF-predicted MAE verified over the 4-km domain area for the 36-km (blue), 12-km (pink) and 4-km (green) grid predictions of the surface layer variables averaged over the 36-h forecast periods for the six Beijing Olympics cases in Table 1. a) wind speed (ms^{-1}), b) wind direction (deg) and c) temperature (C).

boundary layer for the 36-km and 12-km grid resolutions, and MM5 performing better in the boundary layer for the 4-km resolution domain. Although the WRF mean-error statistics (not shown) imply slower wind speeds, subjective analysis of the wind patterns suggested that they were generally similar between the two models. Differences in the model results were related more to differences in the model physics, such as the PBL turbulence schemes as will be shown in the following section.

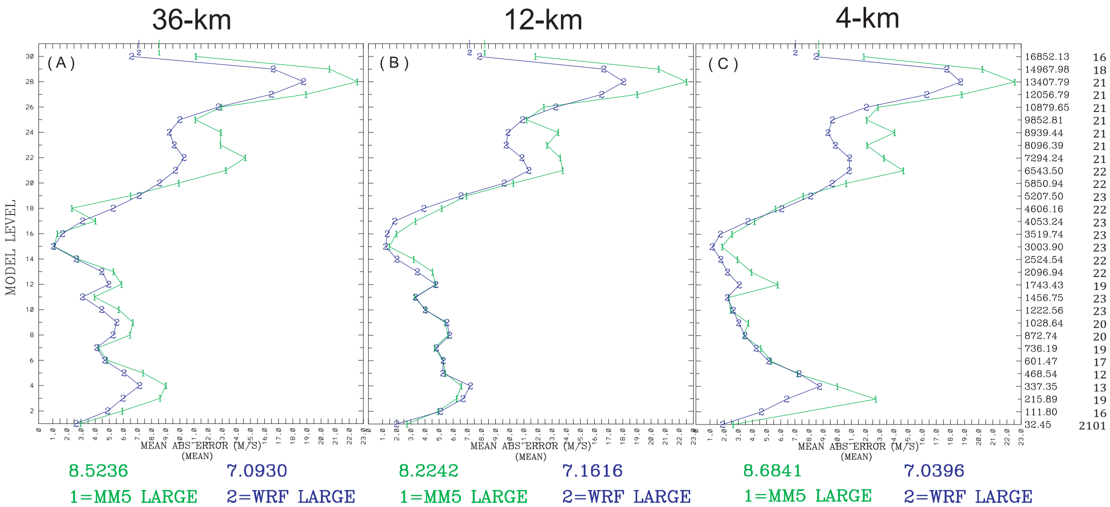

Figure 9. Comparison of MM5- and WRF-predicted MAE wind speed profiles of MAE (ms^{-1}) verified over the 4-km domain area for the 36-km, 12-km and 4-km grid predictions averaged over the 36-h forecast periods for the six Beijing Olympics cases in Table 1. The heights (m, AGL) of the model levels, and the observation counts used in the statistics for each model level are provided on the right hand side of the figure.

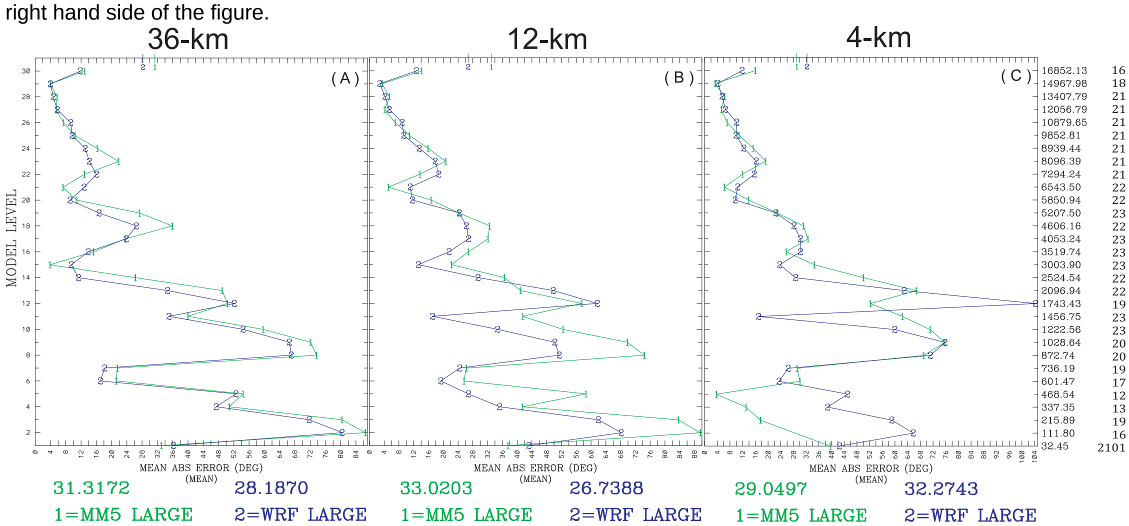

Figure 10. As in Fig. 9 but for wind direction (deg).

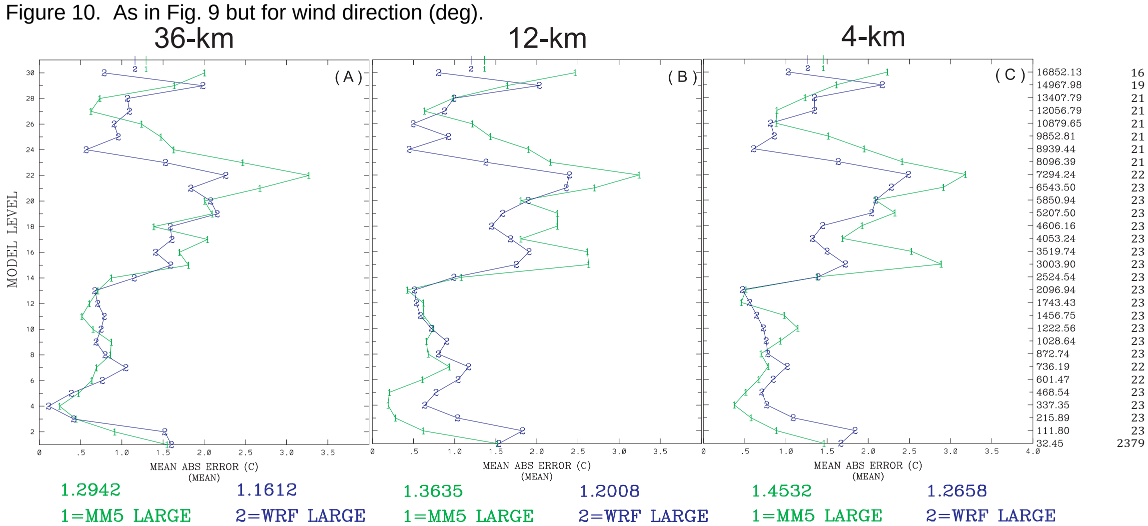

Figure 11. As in Fig. 9 but for temperature (C).

5.2 HPAC-SCIPUFF results for Case 1

Since the low-level meteorology and SCIPUFF results can be sensitive to the predictions for PBL height, our Case 1 comparison of SCIPUFF results for MM5 and WRF includes another MM5 experiment using the M-Y Eta PBL scheme, which is more closely related and more directly comparable to the MYJ PBL scheme in WRF (Table 2). MM5 Eta PBL meteorological results for Case 1 are generally closer to those for WRF with respect to its larger low-level temperature errors and smaller wind speed errors compared to MM5 using the GS PBL scheme (not shown).

Exp. Name	Meteorology MEDOC Input to SCIPUFF	Boundary Layer Type
MM5-GS	MM5 with GS PBL scheme	MM5 MEDOC
MM5-ETA	MM5 with MY Eta PBL scheme	MM5 MEDOC
WRF-MYJ	WRF with improved MYJ PBL scheme	WRF MEDOC

Table 2. Experimental design for the HPAC-SCIPUFF comparison for Case 1 using MM5 vs. WRF weather inputs.

Figure 12 shows that the MM5 using the GS PBL scheme produces the highest daytime PBL depths on average for the 4-km domain for this case, and the MM5 using the MY Eta PBL scheme produces the lowest average daytime PBL depths. The WRF using the MYJ PBL scheme produces average values in between the other two experiments. Note that the daytime SCIPUFF forecasts shown below in this section have releases starting at 24 h, 00 UTC 9 August 2008.

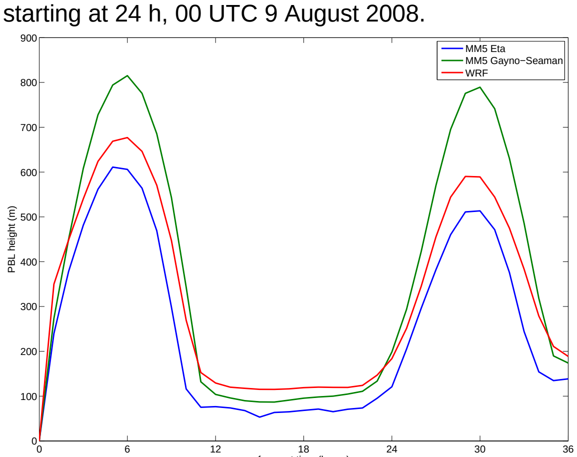

Figure 12. A comparison of model-simulated PBL depth for Case 1, averaged over the entire 4-km Beijing domain, as a function of model hour (starting 00 UTC 8 August 2008 and ending 12 UTC 9 August 2008), for the following experiments: MM5 using the GS PBL scheme (green), MM5 using the MY Eta PBL scheme (blue) and WRF using the modified MYJ PBL scheme (red).

It is shown in Fig. 13 that all three experiments have similar SCIPUFF-predicted surface concentration patterns at 6 h (1400 LST), and that the MM5 using the Eta PBL (lowest average daytime PBL depths) appears to produce the highest surface concentrations, and the MM5 using the GS PBL (highest average daytime PBL depths) produces the lowest surface concentration for all three releases. Although there are no direct observations for SCIPUFF verification, these results are consistent with the predicted and observed surface wind fields in Fig. 2, and they appear to be reasonable because the vertical mixing processes that tend to be stronger (weaker) if the PBL depths are higher (lower),

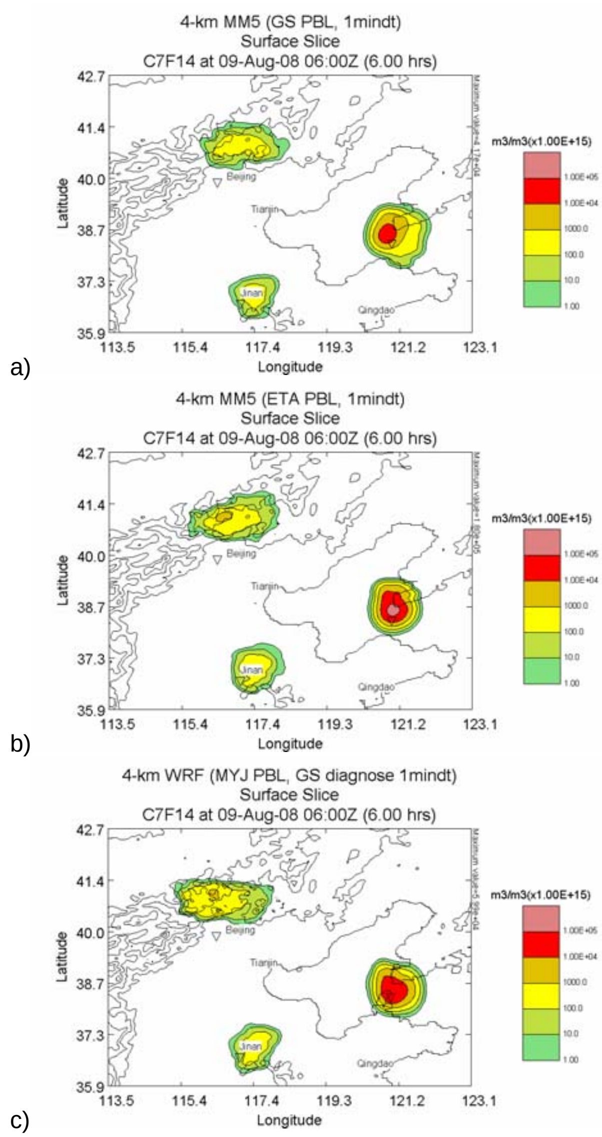

Figure 13. Comparison of SCIPUFF-predicted surface tracer concentrations at 06 UTC (1400 LST) 9 August 2008 (6 h into the SCIPUFF and 30 h into the MM5/WRF forecasts) for the experiments based on the meteorological inputs from a) MM5 using the GS PBL, b) MM5 using the MY Eta PBL and c) WRF using the improved MYJ PBL (Reen et al. 2008, Zielonka et al. 2008).

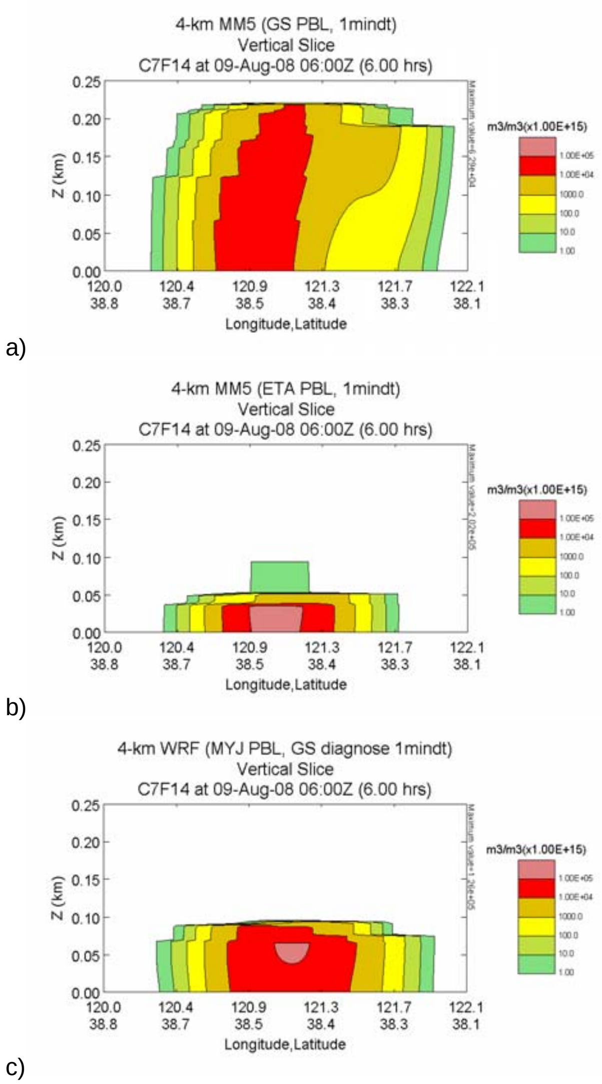

Figure 14. Comparison of SCIPUFF-predicted tracer concentration cross-section (east-west) near the release over the Yellow Sea at 06 UTC (1400 LST) 9 August 2008 (6 h into the SCIPUFF foreacst and 30 h into the MM5/WRF forecasts) for the experiments based on the meteorological inputs from a) MM5 using the GS PBL, b) MM5 using the MY Eta PBL and c) WRF using the modified MYJ PBL.

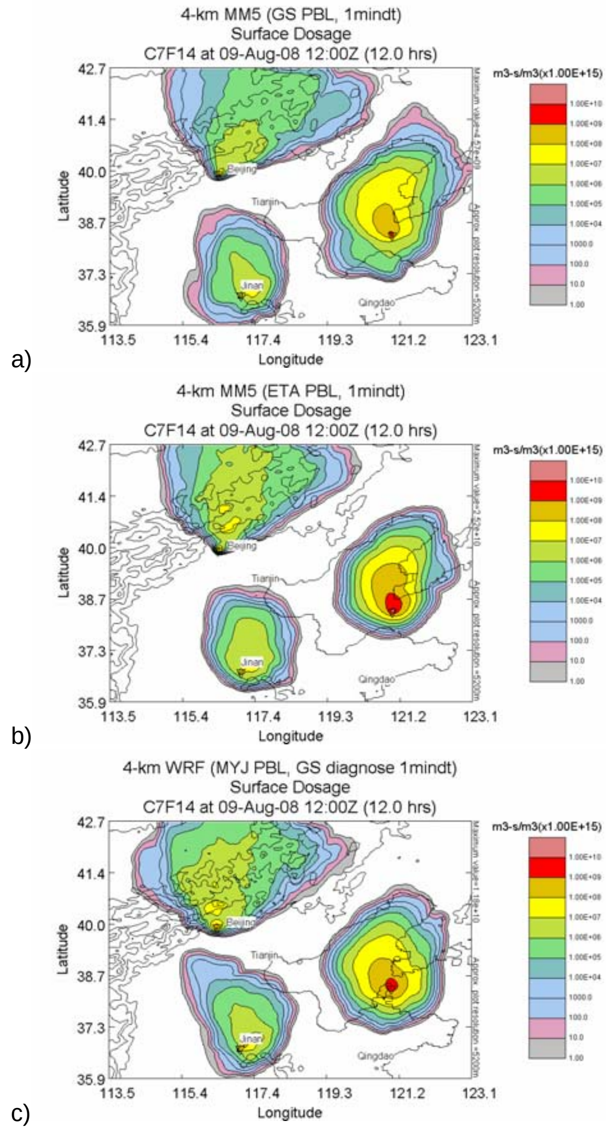

Figure 15. Comparison of 12-h SCIPUFF-predicted surface tracer dosage at 12 UTC (2000 LST) 9 August 2008 (12 h into the SCIPUFF forecast and 36 h into the MM5/WRF forecasts) for the experiments based on the meteorological inputs from a) MM5 using the GS PBL, b) MM5 using the MY Eta PBL and c) WRF using the MYJ PBL.

produce lower (higher) surface concentrations. Comparing the Yellow-sea east-west cross-sections in Fig. 14 at the same time as the surface concentrations in Fig. 13 confirms the conclusions based on the surface concentrations: the MM5-GS plumes extend to higher levels (~200 m) due to stronger vertical mixing, and MM5-Eta plumes are generally confined to a very shallow layer (~50 m), and WRF plumes are found in between (~100 m) the other two experiments.

Figure 15 compares the 12-h surface dosage predictions at this same afternoon time and indicates that all three experiments again have similar concentration patterns, and that the MM5 using the Eta PBL (lowest average daytime PBL depths) appears to produce the highest dosage, and the MM5 using the GS PBL (highest average daytime PBL depths) produces the lowest dosage for all three releases.

6. CONCLUSIONS

The Penn State – DTRA high resolution NWP system or ROFS runs in-house at DTRA and as a development system at Penn State. It has been described and demonstrated using some sample applications (i.e., the Beijing Olympics). The new cluster design and configuration allowed DTRA to create high-resolution meteorological outputs for multiple theaters simultaneously to drive its AT&D models used for hazard prediction and consequence assessment.

The NWP systems were configured to use four domains to create 36-h model forecasts at resolutions as fine as 1.3 km within 6 hours of the GFS model-initialization valid time. It was shown that the model can produce reasonable forecasts for synoptic-scale events such as Hurricane Gustav, while also being able to produce the more localized mesoscale circulations related to sea breezes and downslope flows over different parts of the world. The NWP systems are configured and run on-demand at DTRA in support of their global reachback support.

Results indicate that the MM5 ROFS high-resolution realtime forecasts show very good qualitative and statistical agreement with observations, and the SCIPUFF forecasts based on these model inputs were consistent with the predicted flow fields and PBL structures.

Results also showed that WRF-ARW has improved since our MM5-WRF comparisons for the 2006 Torino Winter Olympics, as both models produced similar results for the 2008 Beijing Summer Olympics. The meteorological forecasts were generally comparable between the MM5 and WRF models with WRF producing somewhat better wind fields, especially for wind speed, and MM5 producing somewhat better thermal fields.

The SCIPUFF predictions for the monsoon/sea-breeze Case 1 based on MM5 and WRF forecast data were also comparable with variations caused by the differences in model-predicted PBL depth. This underlines the importance of accurate representation of PBL depths in the mesoscale NWP models because it is critical for HPAC-SCIPUFF predictions.

7. ACKNOWLEDGMENTS

We acknowledge our NWP systems DTRA contract through Penn State (HDTRA01-03-D-0010) under the supervision of Lt. Col. Charles Harris, Dr. Andy Grose and Mr. Jim Miles, and the research DTRA contract through L-3 Communications to Penn State (DTRA01-03-D-0013-0018) under the supervision of Dr. John Hannan.

8. REFERENCES

Grell, G., J. Dudhia and D.R. Stauffer, 1995: A description of the fifth-generation Penn State/NCAR mesoscale model (MM5). NCAR Tech. Note NCAR/TN-398+STR, 122 pp.

Kain, J.S., 2004: The Kain-Fritsch convective parameterization: An update. *J. Appl. Meteor.,* **43**, 170-181.

Kain, J.S. and J.M. Fritsch, 1990: A One- Dimensional Entraining/Detraining Plume Model and Its Application in Convective Parameterization, *J. Atmos. Sci,* **47**, 2784-2802

Reen, B.P., G.S. Young, D.P. Tyndall, and D.R. Stauffer, 2008: Idealized mesoscale simulations of surface-heterogeneity driven circulations, Preprints, Poster P9.24, W*RF Users' Workshop,* Boulder, CO, June 25, 4 pp.

Schroeder, A.J., D.R. Stauffer, N.L. Seaman, A. Deng, A.M. Gibbs, G.K. Hunter and G.S. Young, 2006: Evaluation of a high-resolution, rapidly relocatable meteorological nowcasting and prediction system. *Mon. Wea. Rev.*, **134**, 1237-1265.

Shafran, P.C., N.L. Seaman, and G.A. Gayno, 2000: Evaluation of Numerical Predictions of Boundary Layer Structure during the Lake Michigan Ozone Study, *J. Appl. Meteor.*, **39**, 412–426.

Stauffer, D.R., G.K. Hunter, A. Deng, J.R. Zielonka, K. Tinklepaugh, P. Hayes and C. Kiley, 2007a: On the Role of Atmospheric Data Assimilation and Model Resolution on Model Forecast Accuracy for the Torino Winter Olympics, Preprints, *22nd Conference on Weather Analysis and Forecasting/18th Conference on Numerical Weather Prediction*, Park City, UT, June 25-29, 7 pp.

Stauffer, D.R., A. Deng, G.K. Hunter, A.M. Gibbs, J.R. Zielonka, K. Tinklepaugh, and J. Dobek, 2007b: NWP Goes to War ..., Preprints, *22nd Conference on Weather Analysis and Forecasting/18th Conference on Numerical Weather Prediction,* Park City, UT, June 25-29, 13 pp.

Stauffer, D.R., R.C. Munoz and N.L. Seaman, 1999: In-cloud turbulence and explicit microphysics in the MM5. Preprints, Ninth PSU/NCAR MM5 Modeling Systems Users' Workshop, Boulder, Colorado, June 23-24, 177-180.

Sykes, R.I., S.F. Parker, D.S. Henn and B. Chowdhury, 2006: SCIPUFF Version 2.2, Technical Documentation, A.R.A.P. Report No. 729, L-3 Titan Corp., Princeton, NJ, 317 pp.

Zielonka, J.R., B.J. Gaudet, N.L. Seaman, D.R. Stauffer, A. Deng, and G.K. Hunter, 2008: WRF and MM5 realtime system statistical comparisons using the Model Evaluation Toolkit (MET), Preprints, *WRF Users' Workshop,* Boulder, CO, June 26, 7 pp.